

Characterization of a quadruple synthetic jet device

Gerardo Paolillo^{1,*}, Carlo Salvatore Greco¹, Gennaro Cardone¹

¹Department of Industrial Engineering, University of Naples, Via Claudio 21, 80125, Naples, Italy
*corresponding author: ger.paolillo@studenti.unina.it

Abstract Synthetic jets are zero-net-mass-flux jets used in numerous applications ranging from flow control to electronics cooling. Synthetic jets offer several advantages, such as small size and no need for an external input piping. As a counterweight they involve problems of acoustic emission because of generally high operating frequencies. In order to reduce noise and increase the heat transfer, multi-jets configurations may be arranged by driving adjacent jets with a phase difference. The present work concerns a quadruple circular synthetic jet actuator. It is made up by four identical speaker-driven cavities, which can act overall as a monopole, dipole or quadrupole acoustic source varying phase relationships between their input signals. In this paper, the necessity of fluid dynamics calibration of such an innovative device is presented and discussed, providing a calibration procedure based on the measurement of the gauge pressure in the cavities by means of differential pressure transducers. Moreover, the flow field generated by the quadruple synthetic jet actuator operating in the monopole-like configuration is investigated by means of phase-locked Stereoscopic PIV. Measurements are carried out at Reynolds and Strouhal number respectively equal to 4300 and 0.184 along a streamwise plane. Phase-average and time-average velocity fields are presented, as a first quantitative and qualitative characterization of the flow field.

Keywords: Synthetic jets, quadruple device, fluid dynamics calibration, Stereoscopic PIV

1 Introduction

A synthetic jet is a zero-net-mass-flux jet generated by the periodic suction and ejection of fluid through an orifice bounding a cavity, due to the oscillatory motion of a diaphragm placed at one of the sides of the cavity. The wide variety of actuators employed as oscillating drivers includes piezoelectric diaphragms [1], pistons [2] and loudspeakers [3]. The diaphragm periodic movement produces a periodic cavity volume variation, thus an internal pressure oscillation. During the suction half of the cycle, the orifice acts as a sink and entrains the near wall fluid into the cavity. On the other hand, during the ejection phase, the flow separates at the edges of the exit section and, under certain operating conditions [4], a vortex ring forms and convects away from the orifice thus forming a time-averaged jet in a limited zone near the jet axis [1].

The dimensionless parameters characterizing synthetic jet flows are the Reynolds number and the Strouhal number defined as:

$$Re = \frac{\rho U_0 D_0}{\mu} \quad (1)$$

$$St = \frac{f D_0}{U_0} = \frac{D_0}{L_0} \quad (2)$$

where U_0 is a characteristic velocity scale, D_0 is the orifice diameter, L_0 is the stroke length and f is the actuation frequency. According to Smith and Glezer (1998), the characteristic velocity U_0 is defined as the mean exit velocity on the jet axis over the ejection half of the cycle:

$$U_0 = \frac{1}{T} \int_0^{T/2} u_a(t) dt \quad (3)$$

where T is the actuation period and $u_a(t)$ is the exit velocity on the jet axis.

In recent years, synthetic jets have been widely investigated by means of different flow visualization techniques and compared to conventional continuous jets. Smith and Glezer [1] studied the formation and evolution of slot (2-D) synthetic jets comparing them to conventional 2-D jets. They observed a higher streamwise decrease of the synthetic jet mean centreline velocity and a lower streamwise increase of its width and of the

volume flow rate. Cater and Soria [2] investigated a round zero-net-mass-flux jet finding that it has a cross-stream velocity distribution similar to that of a conventional continuous jet but with a larger spreading rate and a constant decay.

Unlike conventional continuous jets, synthetic jets do not need injection of additional fluid and a related external piping. This feature, in addition to the consequent small size of synthetic jet actuators, has been the reason of their numerous applications. The experimental and numerical studies of last decades have been focused mainly on two topics: flow control (Amitay et al. [5]; Smith and Glezer [6]; Jabbal and Zhong [7]; Ben Chiekh et al. [8]; Xia and Zhong [9]) and cooling of electronic devices (Mahalingam et al., [10]; Chaudhari et al. [11]; Garimella et al. [12]; Greco et al. [13]). In the field of electronics cooling, synthetic impinging jets offer higher local cooling rates and higher power dissipation in comparison to standard cooling devices, such as fans. Mahalingam et al. [10] studied the effectiveness of a synthetic jet ejector, observing that it dissipates about 40% more power than a conventional fan, at a fixed range of flow rate and for the same configuration. Chaudhari et al. [11] carried out experiments on the cooling of a flat plate by using a synthetic jet generated through a circular orifice. They show that the generated heat transfer is comparable with that of continuous axisymmetric jets at low Reynolds numbers (up to 4000), expecting it to be higher at greater values of the Reynolds number.

In spite of these advantageous features, synthetic jets involve problems of acoustic emission because of generally high operating frequencies. In order to reduce noise, but also to enhance heat transfer, multi-jets configurations may be arranged by driving adjacent jets with a phase difference. Luo et al. [14] proposed a new generation of (2-D) synthetic jet actuators consisting in two cavities sharing the same wall equipped with a single piezoelectric diaphragm and a slide block separating the two exit slots at an appropriate distance. In such a configuration, the diaphragm oscillation produces opposite variations of the volume of the two cavities, which, in fact, act in phase opposition. Lasance et al. [15] realized a twin circular synthetic jets cooling device by splitting one cavity in two identical sub-cavities, both connected to a nozzle, through a loudspeaker. They observed that this device offers heat transfer enhancement and higher power dissipation compared to standard fans, and, in addition, a noise attenuation compared to single jet actuators. Persoons et al. [16], for a fixed operating point and geometry, optimized the cooling performance of twin synthetic jets for phase and jet-to-surface spacing, reaching about 90% enhancement of the maximum and overall cooling rate compared to a single jet, without the need for external cross-flow forcing. Chaudhari et al. [17] realized a particular synthetic jet device by placing satellite orifices around a center orifice, all connected to the same cavity, and investigated its performance. It was shown that the maximum heat transfer coefficient with multiple orifice single-cavity synthetic jets is up to 30% more as compared to that obtained with a conventional single orifice jet. Greco et al. [3] inspected the formation and evolution of twin circular synthetic jets in the near field (half stroke length). Their experimental apparatus was similar to the one of Lasance et al. [15]. Phase-average and time-average PIV measurements were carried out varying the jet axis-to-axis distance for fixed values of the Reynolds and Strouhal numbers. It was observed that for high axis-to-axis distances (3 and 5 diameters) the two adjacent jets exhibit the same features of the single jet configuration; on the other hand, for low axis-to-axis distances (1.1 diameters), it is not possible to discern two separated single synthetic jets and an higher centreline velocity and lower jet width is observed. The latter are a clear evidence of the jets interaction.

The present work focuses on the characterization of an innovative quadruple synthetic jet device. In the first part, the necessity of a fluid dynamics calibration is outlined and discussed, providing a procedure based on cavity pressure measurements. Then, Stereoscopic PIV measurements of the flow field generated by the device acting in the monopole-like configuration are reported in order to give a first quantitative and qualitative characterization of the flow field.

2 Synthetic jet apparatus: geometry and calibration procedure

Fig. 1 shows the schematic of the quadruple synthetic jet actuator. It consists of a center aluminum cubic box, in which four identical elbow pipes are embedded. The nozzle diameter D is 10 mm, the length L_n is about 89.22 mm and the axis-to-axis distance Σ for two adjacent jets is $1.1D$, value for which a fluid interaction between two neighboring jets has been experimentally observed [3]. Each nozzle is connected to a recess in

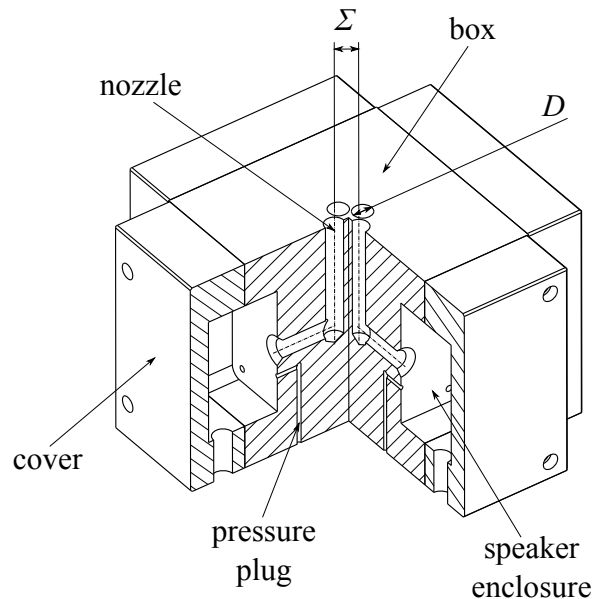


Fig. 1 Quadruple synthetic jet experimental apparatus

one of the side faces of the box, which, assembled with the recess in the correspondent cover, provides the speaker enclosure. When the speaker is screwed on the bottom side of the box recess, the cavity volume V , i.e. the volume delimited by the speaker cone and the wall of the recess, is approximately equal to 8.2 cm^3 .

The speakers used in the present experiments have a diameter of 65 mm, a nominal impedance of 8Ω and maximum input power of 30 W. They are supplied with sinusoidal input signals with the frequency of 120 Hz, generated by Digilent Analog DiscoveryTM USB Oscilloscope coupled with an amplifier. The system is driven by a personal computer and synchronized with the imaging system in order to perform locked phase-average measurements. The operating frequency is set at a value near the lowest resonance frequency of the single actuators.

A single synthetic jet actuator can be modelled as 4th order system, consisting of the coupling between two oscillators: a Helmholtz resonator (cavity and nozzle) and the oscillatory diaphragm (Gallas et al. [18]; Persoons [19]). According to this model, the overall system has two resonance frequencies f_1 and f_2 , related to the natural frequency of the Helmholtz resonator and the resonance frequency of the speaker mounted in an infinite baffle. In literature, semi-empirical formulas for both these frequencies have been proposed [19]. Anyway, in the case of the examined device, the resonance frequencies f_1 of the four actuators were experimentally measured, by determining the mounted speaker impedance curve versus frequency in the range from 50 Hz to 200 Hz.

Fig. 2 illustrates respectively the impedance curves and the difference phase (between the input voltage and current) curves of the four different speakers - designated with the names of the cardinal points - in the case of input voltage amplitude equal to 1 V. The figure shows a discrepancy between the mechanical features of the single actuators, which may result from several factors, such as different manufacturing characteristics or different assembly of the speakers. The resonance frequencies f_1 are not exactly the same but they are all within the range 120-140 Hz. Ultimately, only one actuator can operate at its resonance condition and it's convenient to set the operating frequency at an intermediate value between the four resonance frequencies f_1 . However, the operating frequency must also satisfy the synthetic jet formation criterion [4] and match an appropriate value of the Strouhal number (or equally the stroke length).

As a consequence of the different mechanical behaviour of the single actuators, the jets synthesized when they are supplied with the same input signal, have different features and so a fluid dynamics calibration is necessary to make jets work at the same operating point (Reynolds number and stroke length) and to implement the several device configurations in an appropriate way.

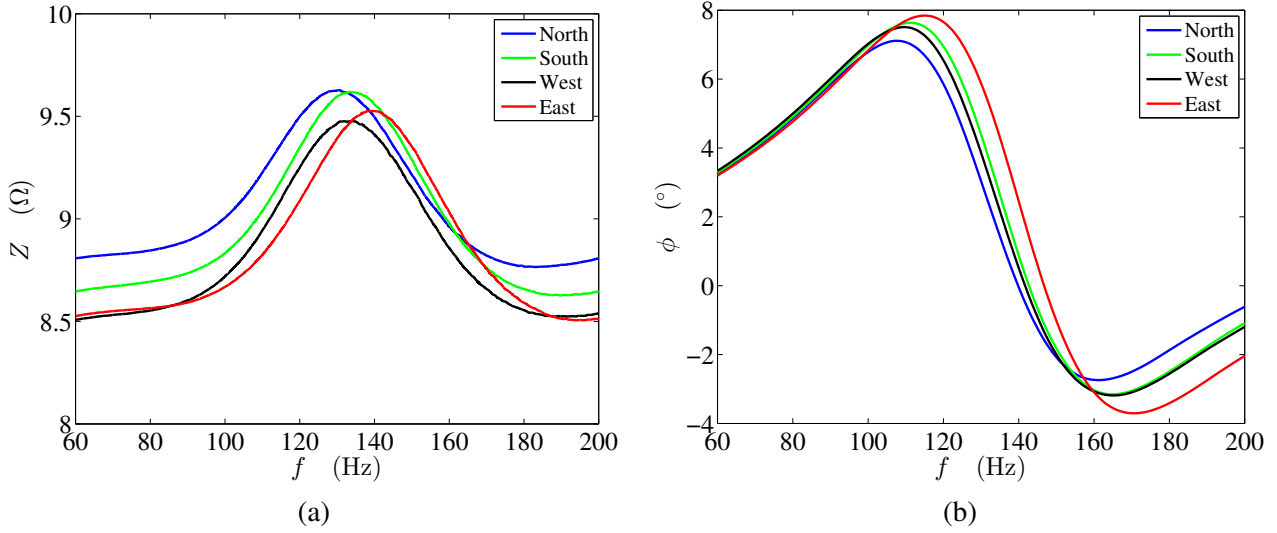


Fig. 2 Impedance (a) and phase angle (b) for the mounted speakers. Amplitude of the input voltage signal: $V_{in} = 1$ V; initial phase angle of the input: $\phi_{in} = 0^\circ$.

The calibration aims to determine the waveform of the sinusoidal voltage signals to be sent to the speakers, in terms of amplitude and initial phase angle (the frequency is fixed), in order to obtain pressure oscillations in the four cavities identical to each other, except for an appropriate phase difference. The latter condition ensures that the jets have identical exit velocity and pressure, independently from characteristics of the speakers which have generated them, since the four resonant cavities and nozzles have the same geometry and dimensions and so the correspondent pressure losses are expected to be the same.

The calibration is based on the measurement of the gauge pressures in the cavities, performed by means of differential pressure transducers (Honeywell SSCDRR020NDAA5) connected to the pressure plugs of the cavities. The procedure starts taking one cavity as reference and determining the pressure response of this cavity to an input voltage signal of assigned amplitude and initial phase angle (in the present experiment, $V_{ref} = 1.2$ V and $\phi_{ref} = 0^\circ$); then, an iterative process allows to determine the amplitude ratios and phase lags between the input signal of the reference actuator and the input signals to be sent to the other actuators in order to obtain pressure responses of the correspondent cavities identical to that of the reference cavity.

The cavities are calibrated one at a time. The process of calibration of a single cavity consists of two successive steps: the amplitude calibration and the phase calibration. Each of these phases, in fact, involves an iterative process.

At each iteration of the amplitude calibration, at first, the pressure response to a specific input signal with a fixed duration - multiple of the actuation period T - is determined by repeating the measurement for 500 times and calculating the mean, thus reducing random error (at the first iteration, the input signal coincides with the input signal of the reference actuator). Then, the ratio ρ between the amplitude of the pressure response of the reference cavity p_{ref} and the amplitude of the pressure response of the considered cavity p_{cal} is calculated as ratio between the averages of the absolute value of these pressures over the period:

$$\rho = \frac{\bar{P}_{ref}}{\bar{P}_{cal}} \quad (4)$$

where the symbol \bar{P} indicates the average of the absolute value of the pressure over the period:

$$\bar{P} = \frac{1}{T} \int_0^T |p(t)| dt. \quad (5)$$

If $\rho < 1 - \epsilon$ with $\epsilon = 0.005$, the procedure is stopped; otherwise, the amplitude of the input signal is modified by multiplying it by ρ itself and a new iteration is performed. The cycle continues until the stopping criterion is satisfied.

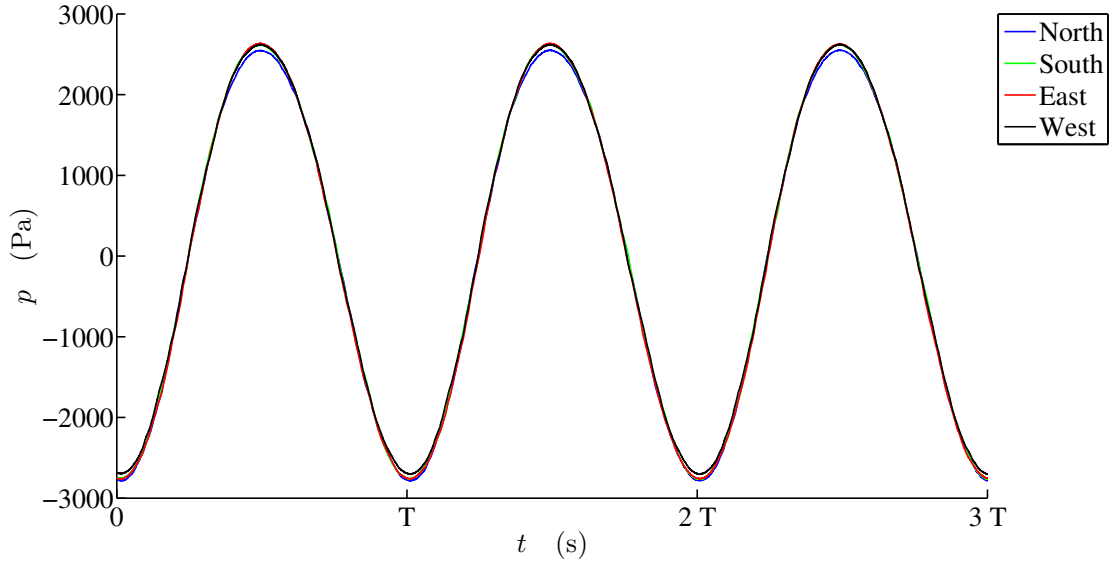


Fig. 3 Pressure responses of the cavities to the input voltage signals after calibration. The actuation period is $T = 1/f = 1/120$ s, the amplitude of the input signal of the reference actuator (*East*) $V_{\text{ref}} = 1.2$ V.

After the amplitude calibration, the phase calibration can start. At each iteration, the phase lag $\Delta\phi$ between the pressure response of the examined cavity and the pressure response of the reference cavity is estimated by determining the phase shift which maximizes the cross-correlation between the two signals. Then, the initial phase angle of the input signal is increased by $\Delta\phi$; the pressure response of the cavity is recorded again (the measurement is still repeated for 500 times) and the new value of phase lag $\Delta\phi$ is determined. The cycle is stopped when $\Delta\phi < \delta$, where $\delta = 0.036^\circ$.

It should be noted that, for both calibrations, a single iteration could be not sufficient because of the non-linear relationship between the pressure response (amplitude and initial phase angle) and the input signal. In addition, the speaker impedance depends on the excitation voltage amplitude. In particular, the acoustic impedance of the air in the speaker enclosure (which combines with the electrical impedance and inertia of the speaker itself) depends on the mean pressure in the enclosure. Such a mean pressure varies with the membrane displacement amplitude and so with the input amplitude. On the contrary, the mechanical features of the actuators are independent of the input initial phase angle and this justifies the possibility of performing the phase calibration after the amplitude calibration. For the same reasons, the calibration can not be based on the impedance curves and the phase angle curves of the speakers.

The Fig. 3 shows the gauge pressure responses of the cavities to the correspondent inputs after the amplitude and phase calibration.

3 Stereoscopic PIV experimental setup

As quadruple synthetic jet flow is expected to be strongly 3D, stereoscopic PIV is used to measure three-component velocity in the most significant streamwise planes of each investigated configuration. The experimental apparatus is shown in fig. 4.

The flow is seeded with oil droplets with a nominal diameter of $1 \mu\text{m}$. The particles are illuminated with a Quantel Evergreen laser (Nd-YAG, 200 mJ/pulse). Appropriate spherical and cylindrical lenses and mirrors are employed to create a 1 mm light sheet. The time delay between the two laser pulses is set to $50 \mu\text{s}$.

Images of the flow are acquired by two Andor Zyla cameras (sCMOS sensors of 2560×2160 pixels) equipped with 50 mm focal length lens. The cameras have a relative aperture of $f_{\#1} = 5.6$ (Camera 1) and $f_{\#2} = 8$ (Camera 2). The angle between the optical axes of the two cameras is set at about 50° and Scheimpflug adapters are used in order to achieve good focus over the entire field of view. The spatial resolution of two cameras is estimated to be $100 \mu\text{m}/\text{px}$. The field of view extends from 0.8 diameters to 20.2 diameters downstream of the exit plane of the nozzles along the streamwise direction, and over 18.8 diameters along the spanwise

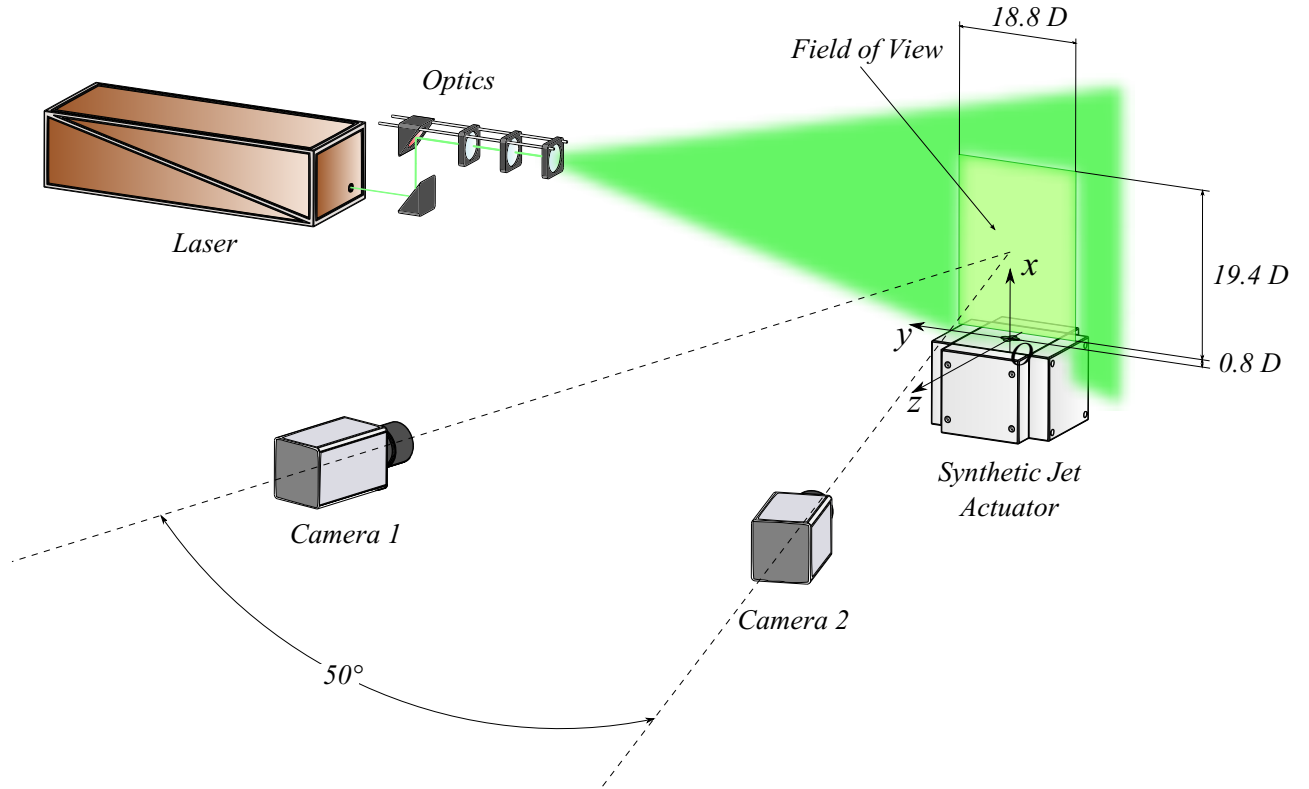


Fig. 4 Stereoscopic PIV experimental apparatus

direction.

In order to obtain reliable mean velocity field over the period, 90 phases of the oscillation are sampled. That is possible by sampling the phenomenon every $n + 1/NDiv$ period of the membrane oscillation (n is a natural number, $NDiv$ the number of sampled phases) with an appropriate frequency f_s . In particular, the latter is related to the actuation frequency f and n by the following equation:

$$f_s = \frac{f}{\frac{1}{NDiv} + n}. \quad (6)$$

4 Results and discussion

In the present experiments, only the monopole-like configuration is investigated. Measurements are carried out at Reynolds and Strouhal numbers respectively equal to 4300 and 0.184 along the streamwise plane passing through the axes of two opposite nozzles (*North* and *South*). For each phase (90 in total), 50 double-frame images are acquired for a total of 4500 images.

In Fig. 5 the mean axial flow field is shown. It is possible to observe that the four synthetic jets (in the measurement plane only two are visible) merge very close to the nozzle exit plane. After the merge, a contraction and a subsequent expansion of the jet thickness are clearly visible. Then, the four synthetic jets start acting like a single synthetic jet. Indeed, the highest axial velocity is located on the middle axis ($y = 0$) between the two observed jets.

Fig. 6 presents the variation of the centreline mean velocity U_c and the jet width b along the streamwise direction. The jet width b is defined as the distance between the two spanwise y positions where the axial mean velocity is half of the centreline mean velocity.

As regards the centreline mean velocity U_c , three different regions of the synthetic jet can be detected. The first is characterized by an abrupt increase of U_c from the exit plane of the nozzles (where the average velocity

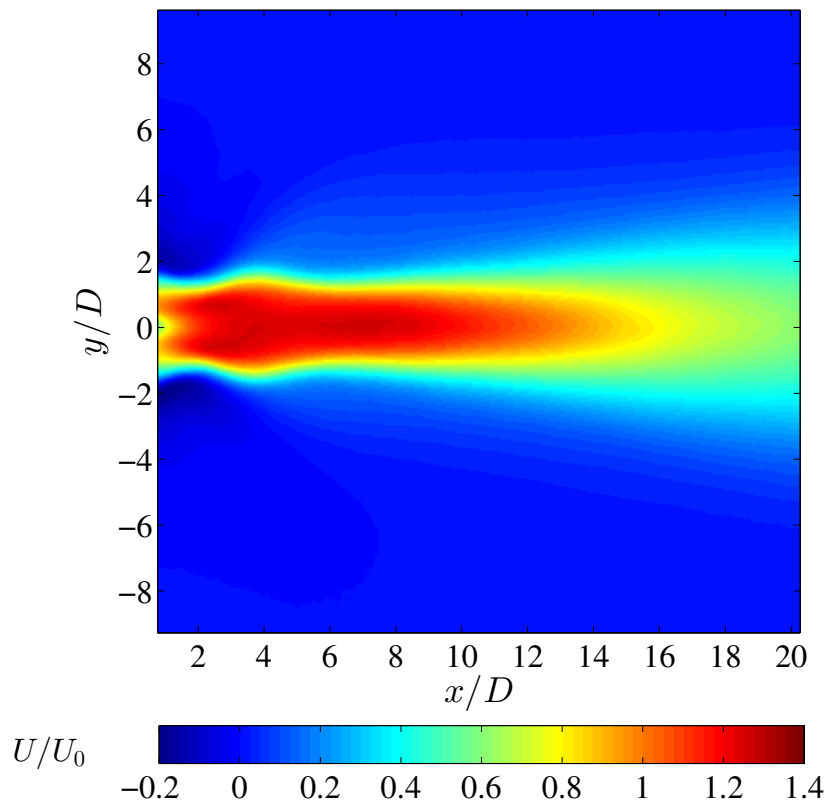


Fig. 5 Time-average flow field for the monopole-like configuration along the streamwise “North-South” plane. $Re = 4300$, $Sr = 0.184$

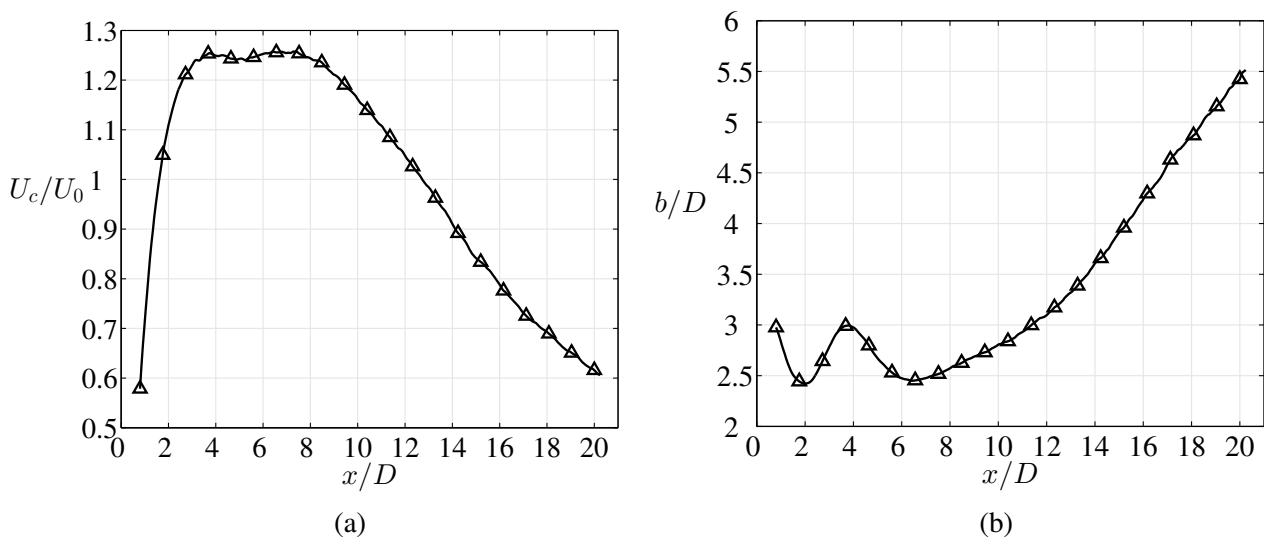


Fig. 6 (a) Normalized jet centreline velocity, (b) non dimensional jet width evolution for the monopole-like configuration. $Re = 4300$, $Sr = 0.184$

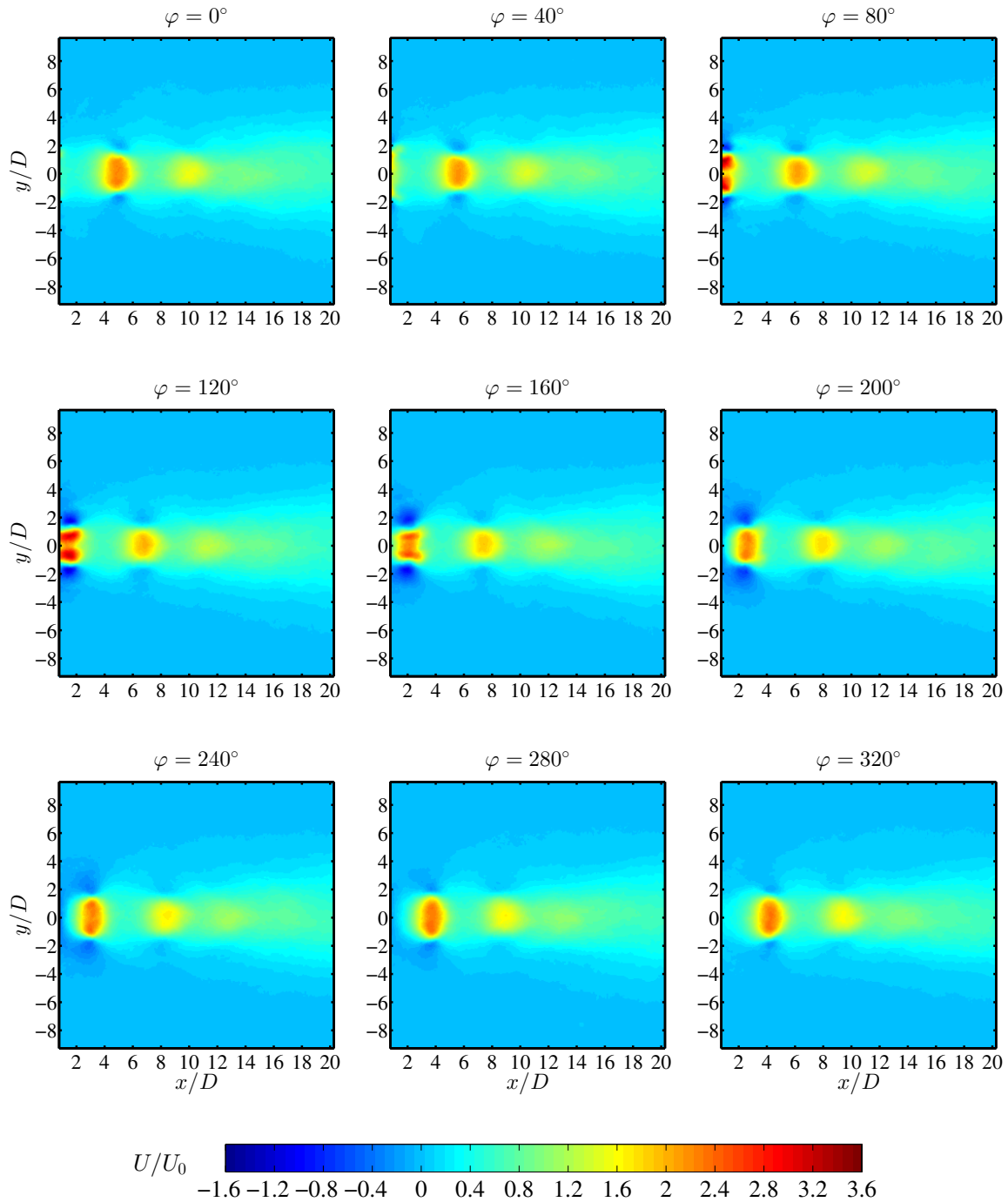


Fig. 7 Phase-average flow field for the monopole-like configuration along the streamwise “North-South” plane. $Re = 4300$, $Sr = 0.184$

should obviously be equal to zero) up to $x/D = 2.05$. This abrupt increase is due to the merge of the four synthetic jets. In the middle region, $2.05 < x/D < 7.8$, the velocity profile is approximately constant. Such a plateau has a value which is higher than that attained by a single synthetic jet (i.e. about $1.1 U_0$). In the last region the velocity decays and, at the end of the field of view, $x/D = 20.2$, it is about the half of the maximum value.

Fig. 6 (b) shows that the jet width has an irregular behaviour. At first, it decreases up to about $x/D = 2$ because of the merge of the four synthetic jets. After that, the jet width increases up to x/D equal to 3.8 and then decreases again up to $x/D = 6.4$. Only after such a oscillating behaviour the jet width curve shows a positive slope resembling that of a single synthetic jet.

Fig. 7 illustrates the evolution of the flow field over the entire period. Only 9 phases are presented starting from $\varphi = 0^\circ$ up to $\varphi = 320^\circ$. The phase $\varphi = 0^\circ$ corresponds to the beginning of the ejection phase of the four jets. At this phase, it is possible to observe two vortex structures whose cores are located respectively at about $x/D = 5$ and $x/D = 10$. The spacing between these structures (about five diameters) has the same value of the dimensionless stroke length. As matter of fact, according to Shuster and Smith [20], the vortex ring displacement is proportional to the stroke length.

It is worth noting that the velocity of the first vortex structure (on the left) is higher than the second one (on the right). This is due to the fact that the vortex structure is undergoing to transition. Indeed about five diameters downstream of the second vortex ring, any clearly visible coherent vortex structure can't be detected. Furthermore, it has to be pointed out that each detected vortex structure is not simply a single vortex ring, but the section of more complex coherent structure resulting from the interaction of four different vortex rings.

As the exit velocity increases (i.e. φ increases), these vortices move away from the nozzle exit plane and gradually weaken. At the phases $\varphi = 40^\circ$ and $\varphi = 80^\circ$ it's possible to discern the two separate synthetic jets, but they are so close to each other that the internal footprint of the vortex ring is not detectable. This could be related to a destructive interference between the two internal vortex ring footprints which have an opposite sign. At $\varphi = 120^\circ$ the two jets start merging and a complete coalescence is reached only at $\varphi = 200^\circ$. At this phase only a vortex structure, resembling the vortex ring issued by a single synthetic jet device, can be observed. As φ further increases, such a vortex structure convects downstream and dissipates.

The presence of the two vortices in the near field during the entire cycle is the reason why the mean jet width presents the particular variation shown in Fig. 6, characterized by two local minima at the stations $x/D = 2$ and $x/D = 6.4$ (which are related to the locations of the two cores over the period) and a local maximum at $x/D = 3.8$ (which is due to the jet spread downstream of the first vortex before being entrained into the center region of the successive one).

5 Conclusions

In the present work, an innovative quadruple synthetic jet device has been presented. This device has been designed in order to reach a noise reduction and a heat transfer enhancement in comparison with conventional synthetic jet actuators. Before performing acoustic and heat transfer studies, a first characterization of such a device has been carried out through PIV measurements.

First of all, the necessity of a fluid dynamics calibration of this innovative device has been presented and discussed, providing, in addition, a calibration procedure based on the measurement of the gauge pressure in the cavities by means of differential pressure transducers. Both the amplitude calibration and the phase calibration enable to manage the device in a correct way, that is in such a way as to implement those operating configurations which could lead to an effective improvement in the acoustic and the heat transfer performance. The results of the calibration, in terms of the pressure response of the cavities, have been reported, thus showing the effectiveness of the designed procedure.

In the second part of the paper, the results of the phase-locked Stereoscopic PIV investigation are presented. Only the flow field generated by the quadruple synthetic jet actuator operating in the monopole-like configuration has been studied. Measurements have been carried out at Reynolds and Strouhal number respectively equal to 4300 and 0.184 along a streamwise plane. Some characteristic parameters of this flow field, as the jet centreline and the jet width, have been presented and the time-average and phase-average flow field of the axial velocity have been shown. The flow field behaviour has been discussed and its evolution, through the phase-average measurements, has been described. The four synthetic jets merge very close to the nozzle exit plane generating a coherent vortex structure, which affects the jet width and velocity centreline behaviour.

After this first quantitative and qualitative characterization of the flow field, different configurations (dipole, quadrupole and etc.) will be experimentally studied, performing not only PIV measurements but also acoustic and heat transfer ones.

References

- [1] Smith B L, Glezer A (1998) The Formation and Evolution of Synthetic Jets. *Physics of Fluids*, vol.10, n° 9, pp 2281-2297. doi: 10.1063/1.869828
- [2] Cater E, Soria J (2002) The evolution of round zero net mass flux jet. *Journal of Fluid Mechanics*, vol. 472, pp 167-200. doi: 10.1017/S0022112002002264
- [3] Greco C S, Ianiro A, Astarita T, Cardone G (2013) On the near field of single and twin circular synthetic air jets. *International Journal of Heat and Fluid Flow*, vol. 44, pp 41-55. doi: 10.1016/j.ijheatfluidflow.2013.03.018
- [4] Holman R, Utturkar Y, Mittal R, Smith B L, Cattafesta L (2005) Formation Criterion for Synthetic Jets. *AIAA Journal*, vol. 43, pp 2110-2116. doi: 10.2514/1.12033
- [5] Amitay M, Smith D R, Kibens V, Parekh D E, Glezer A (2001) Aerodynamic flow control over an unconventional airfoil using synthetic jet actuators. *AIAA Journal*, vol. 39, pp 361-370. doi: 10.2514/2.1323
- [6] Smith B L, Glezer A (2002) Jet vectoring using synthetic jets. *Journal of Fluid Mechanics*, vol. 458, pp 1-34. doi: 10.1017/S0022112001007406
- [7] Jabbal M, Zhong S (2008) The near wall effect of synthetic jets in a boundary layer. *International Journal of Heat and Fluid Flow*, vol. 29, pp 119-130. doi: 10.1063/1.3432133
- [8] Ben Chiekh M, Ferchichi M, Bérac J C (2011) Modified flapping jet for increased jet spreading using synthetic jets. *International Journal of Heat and Fluid Flow*, vol. 32, pp 865-875. doi: 10.1016/j.ijheatfluidflow.2011.06.004
- [9] Xia Q, Zhong S (2012) A PLIF and PIV study of liquid mixing enhanced by a lateral synthetic jet pair. *International Journal of Heat and Fluid Flow*, vol. 37, pp 64-73. doi: 10.1016/j.ijheatfluidflow.2012.04.010
- [10] Mahalingam R, Rumigny N, Glezer A (2004) Thermal management using synthetic jet ejectors. *IEEE Transactions on Components and Packaging Technologies*, vol. 27, issue 3, pp 439-444. doi: 10.1109/TCAPT.2004.831757
- [11] Chaudhari M, Puranik B, Agrawal A (2010) Heat transfer characteristics of synthetic jet impingement cooling. *International Journal of Heat and Fluid Flow*, vol. 53, pp 1057-1069. doi: 10.1016/j.ijheatmasstransfer.2009.11.005
- [12] Garimella S V, Yeh L-T, Persoons T (2012) Thermal management challenges in telecommunication systems and data centers. *IEEE Transactions on Components, Packaging and Manufacturing Technology*, vol. 2, pp 1307-1316. doi: 10.1109/TCPMT.2012.2185797
- [13] Greco C S, Ianiro A, Cardone G (2014) Time and phase average heat transfer in single and twin circular synthetic impinging air jets. *International Journal of Heat and Mass Transfer*, vol. 73, pp 776-788. doi: 10.1016/j.ijheatmasstransfer.2014.02.030
- [14] Luo Z B, Xia Z X, Bing L (2006) New generation of synthetic jet actuators. *AIAA Journal*, vol. 44, n° 10, pp 2418-2419. doi: 10.2514/1.20747
- [15] Lasance C J M, Aarts R (2008) Synthetic jet cooling part I: Overview of heat transfer and acoustic. In: Proceeding of the 24th Annual IEEE Semiconductor Thermal Measurement and Management Symposium, pp 20-25. doi: 10.1109/STHERM.2008.4509360
- [16] Persoons T, O'Donovan T S, Murray D B (2009) Heat transfer in adjacent interacting impinging synthetic jets. In: ASME 2009 Heat Transfer Summer Conference (HT2009), July 19-23, San Francisco, pp 955-962. doi: 10.1115/HT2009-88440
- [17] Chaudhari M, Puranik B, Agrawal A (2011) Multiple orifice synthetic jet for improvement in impingement heat transfer. *International Journal of Heat and Fluid Flow*, vol. 54, pp 2056-2065. doi: 10.1016/j.ijheatmasstransfer.2010.12.023
- [18] Gallas Q, Holman R, Nishida T, Carroll B, Sheplak M, Cattafesta L (2003) Lumped element modeling of piezoelectric-driven synthetic jet actuators. *AIAA Journal*, vol. 41, pp 240-247. doi: 10.2514/2.1936

- [19] Persoons T (2012) General reduced-order model to design and operate synthetic jet actuators. *AIAA Journal*, vol. 50, pp 916-927. doi: 10.2514/1.J051381
- [20] Shuster J M, Smith D R (2007) Experimental study of the formation and scaling of a round synthetic jet. *Physics of Fluids*, vol.19, issue 4, article number 045109. doi: 10.1063/1.2711481